Materials Science in Semiconductor Processing 24 (2014) 126–131

Contents lists available at ScienceDirect

Materials Science in Semiconductor Processing

journal homepage: www.elsevier.com/locate/mssp

in situ synthesis of graphene/SnO_2 quantum dots composites for chemiresistive gas sensing

K.R. Nemade, S.A. Waghuley *

Department of Physics, Sant Gadge Baba Amravati University, Amravati 444 602, India

ARTICLE INFO

Keywords:
Chemiresistor
Graphene
Quantum dots

ABSTRACT

Chemiresistors based on graphene/SnO_2 quantum dots composites have been fabricated for low temperature detection of liquefied petroleum gas (LPG). Because of the flammable nature of LPG, this investigation focused on the detection of LPG at low temperatures, in order to find a cost-effective and low risk detection method. The structural, morphological, and optical characterization of synthesized composites was done using X-ray diffraction, field emission-scanning electron microscopy, transmission electron microscopy, UV-visible and fluorescence spectroscopy. The as-obtained composites show significantly better performance for the detection of LPG. The sensing mechanism used defects chemistry.

1. Introduction

Liquid petroleum gas (LPG) is a clean fuel with a high octane number and is suited for use in vehicles with both in terms of emissions and cost of the fuel. The main advantage of using automotive LPG is that it is free of lead and has a very low concentration of sulfur. Moreover, LPG is not a greenhouse gas. LPG forms an explosive mixture with air at concentrations between 2% and 10%. This is considerably narrower than other common gaseous fuels. Therefore LPG vapors which can collect in low-lying areas in the eventuality of the leakage are hazardous [1]. The auto-ignition temperature of LPG is ~683–853 K and hence it is necessary to be able to detect LPG at low temperatures [2].

Photo-acoustic spectroscopy has been proposed as a successful option for gas detection with high sensitivity and good selectivity with the possibility of non-destructive analysis. These attributes make photo-acoustic spectroscopy a powerful analytical tool for monitoring of gases [3]. However, some serious limitations also are associated with spectroscopy, e.g. the source of energy must be sufficient (10 $\mu W/cm^2$), the window of the sampling cell must be transparent, and background noise can hamper the acoustic measurements. Besides those limitations, it is a very expensive technique for monitoring of gases [4]. Compared with photo-acoustic spectroscopy, chemiresistive detection of gases is a more straightforward and cost effective technique [5–9].

LPG sensors using semiconducting metal oxides are the most promising for the detection of LPG because of their high sensitivity, low cost, and the possibility of continuous monitoring [10–12]. However, a disadvantage of this LPG sensor was low selectivity [13,14]. Choi et al. have fabricated a nanowire-based gas sensor using a simple method of growing SnO_2 nanowires. The gas sensing performance of this sensing material was demonstrated using diluted NO_2. The sensitivity, as a function of temperature, was highest at 473 K [15].

Thus, great attention has been recently paid to development of new material for LPG gas sensing. Therefore, the goals for this research are to produce a reliable, highly selective, and sensitive LPG sensing material. Hence, the

* Corresponding author. Tel.: +91 9423124882; fax: +91 7212662135.
E-mail address: sandeepwaghuley@sgbau.ac.in (S.A. Waghuley).

http://dx.doi.org/10.1016/j.mssp.2014.02.047
1369-8001/

present work comprises a bold attempt to develop a chemiresistor based upon unattempted graphene/SnO_2 composite as the sensing material.

Li et al. have previously reported the synthesis of graphene/SnO_2 nanocomposites for application as electrochemical supercapacitors [16]. Zhang et al. have examined the H_2S sensing applications of highly aligned SnO_2 nanorods on graphene three-dimensional (3D) array structures synthesized by a straightforward nanocrystal-seeds-directing hydrothermal method [17]. Song et al. have demonstrated a cataluminescence gas sensors application of graphene sheets decorated with SnO_2 nanoparticles, synthesized by hydrothermal assisted an *in situ* synthesis route [18]. A new simple route to prepare N-doped graphene-SnO_2 sandwich papers was developed by Wang et al. for high-performance lithium-ion batteries [19]. Wang et al. have also reported graphene-supported SnO_2 nanoparticles prepared by a solvothermal approach for enhanced electrochemical performance in lithium-ion batteries [20]. Lian et al. have reported a gas–liquid interface synthesis approach, which has been developed to prepare SnO_2/graphene nanocomposites and focused on the high reversible capacity of SnO_2/graphene nanocomposites as anode materials for lithium-ion batteries [21].

Therefore, in this work, we fabricated graphene/SnO_2 chemiresistors for LPG sensing and studied its defects-based mechanism. Some crucial accomplishments are reported; e.g. the chemiresistors have high sensing response and selectivity, low operating temperature, fast response and recovery, and good stability.

2. Experimental

In the present work, we adopted a convenient *in situ* method to prepare graphene/SnO_2 quantum dots (QDs) composites. All chemicals were of analytical grade and used as received, without further purification. The preparation of graphene/SnO_2 QDs composites can be divided into three steps. First, in two separate beakers, $SnCl_4$ and NaOH dissolved in deionized water of resistivity not less than 18.2 MΩ.cm with a molar ratio of 1:4. The solution was put in an ultrasonic bath for 2 h. Second, graphene was mixed in solution placed in oven to dry at 373 K. The graphene samples used in this study were prepared by a previously reported method [22]. Accordingly, four samples were prepared by altering the proportion of graphene from 0.4 to 1.6 wt.%. Third, the dried products were sintered in a quartz tube at 473 K for 8 h under a nitrogen atmosphere.

The X-ray diffraction patterns were obtained using a Rigaku (Miniflex II, Japan) diffractometer with CuKα radiation in the range 10°–70°. The morphology of the sample was observed using field emission-scanning electron microscopy (FE-SEM) and transmission electron microscopy (TEM) using JEOL JSM-7500F and (JEOL-1200ex, Japan) equipment, respectively. The UV-visible analysis was performed on a Perkin Elmer UV spectrophotometer in the range 200–400 nm. The fluorescence measurement was done using an FL spectrophotometer (Model: Hitachi, F-7000, Japan).

The chemiresistors of as-prepared samples were fabricated by a screen-printing technique on a 25 mm × 25 mm glass substrate using a temporary binder (composed of butyl carbitol and ethyl cellulose). For the gas sensing measurements, ohmic contact was achieved using high-conducting silver paint deposited on adjacent sides of the chemiresistor and annealing the chemiresistors at 373 K for 30 min in argon. The average thickness of the screen-printed layer was ~9 μm, measured using a Digimatic Outside Micrometer (Series-293, Japan). In order to test the gas sensing ability of chemiresistors, the gas sensor unit was specially designed.

The sensing response of the chemiresistors was analyzed at different concentrations (ppm) and temperatures. The gas concentration required inside the 5-l chamber was maintained by injecting a known volume of test gas using gas-injection syringes of different volumes. The concentration inside the chamber was increased by adding a particular amount of gas. During this experiment, the resistance of the chemiresistor was measured using the voltage drop method [23]. All measurements were carried out using dry air as the carrier gas having a H_2O content lower than 2 ppm. The sensing response of the chemiresistor is defined as the ratio of resistance in the gas–air mixture to the stabilized resistance in air and is given in Eq. (1) [24]:

$$S = \frac{\Delta R}{R_a} = \frac{|R_g - R_a|}{R_a}. \quad (1)$$

where R_a and R_g is the resistance of the chemiresistor in air and gas, respectively.

3. Results and discussion

3.1. Materials characterization

Fig. 1a–d shows XRD patterns of the as-prepared graphene/SnO_2 QDs composites. From the XRD patterns, it

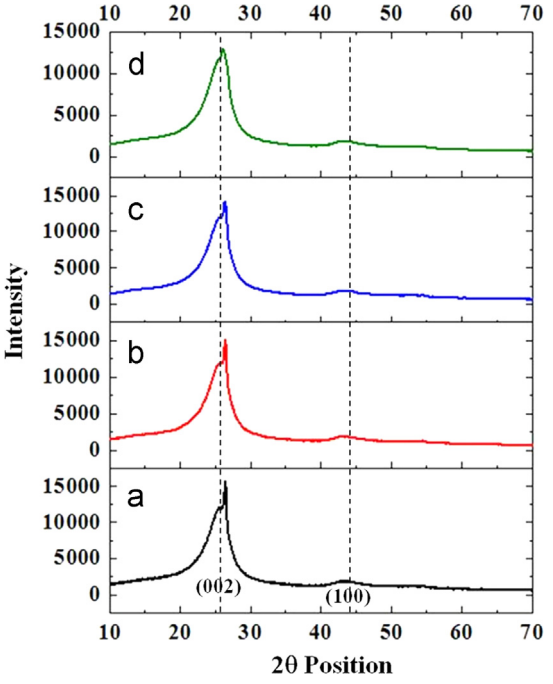

Fig. 1. XRD patterns of (a) 0.4 wt.%, (b) 0.8 wt.% (c) 1.2 wt.% and (d) 1.6 wt.%, of graphene/SnO_2 QDs composites.

can be seen that two peaks, (0 0 2) and (1 0 0) appear prominently, and these are the characteristic peaks of graphene [25]. Moreover, it can be seen also that the intensities of the XRD peaks of the SnO_2 QDs weakened. This indicates that the SnO_2 average grain dimension is smaller than that of the graphene. By using Scherrer's formula, the average grain size is ranges between 4 and 8 nm. The shoulder peak appears at $2\theta = 27^\circ$ and is a characteristic peak of SnO_2. The intensity associated with this peak decreased significantly with increased wt.% of graphene.

In order to shed light on the morphology, FE-SEM and TEM analysis was performed. The FE-SEM image in Fig. 2a clearly shows the typical morphology of the as-obtained product for 1.6 wt.% graphene/SnO_2 QDs composites. This product comprised QDs with the sizes of ~4–8 nm. The FE-SEM micrograph also indicates that SnO_2 QDs are exclusively deposited on the graphene sheets with high density and high uniformity. These SnO_2 QDs are firmly attached to the graphene sheets. As shown in the TEM image (Fig. 2b), many SnO_2 QDs with diameters of 2–4 nm are attached to the corner of the graphene sheets. Tiny SnO_2 QDs are found anchored on this graphene.

UV-VIS spectra of the as-synthesized graphene/SnO_2 QDs composites is shown in Fig. 3. It is observed that the samples have a strong absorption peak within the range of 203–206 nm. The particle size distribution of SnO_2 QDs

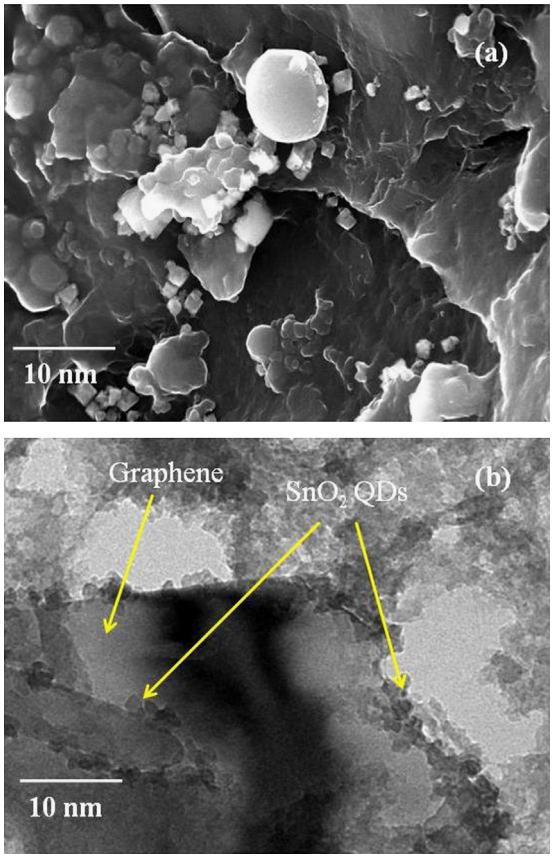

Fig. 2. (a) FE-SEM and (b) TEM image of 1.6 wt.% graphene/SnO_2 QDs composite.

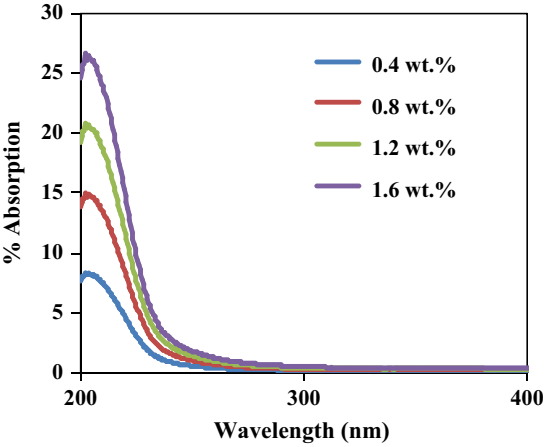

Fig. 3. UV–visible absorption spectrum of the as-synthesized composites.

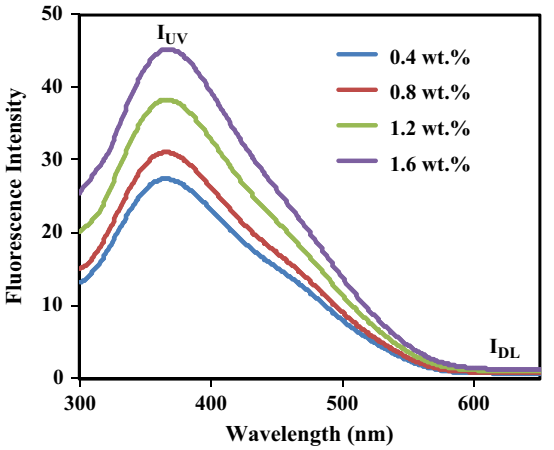

Fig. 4. Fluorescence spectrum of the as-synthesized composites.

Table 1
I_{UV}, I_{DL} and (I_{UV}/I_{DL}) ratio values for graphene/SnO_2 QDs composites.

Sample	I_{UV}	I_{DL}	(I_{UV}/I_{DL}) Ratio
0.4 wt.%	26.92	1.33	20.240
0.8 wt.%	30.97	1.33	23.285
1.2 wt.%	37.86	1.33	28.466
1.6 wt.%	45.22	1.33	34

was found to be in the range of 2–4 nm, with absorption in UV region, which clearly confirmed the presence of a strong quantum confinement effect [26,27].

Sensing properties are strongly affected by the defects concentration. The defect concentration can be estimated by using the fluorescence intensity ratio between the ultraviolet (I_{UV}) and visible deep levels (I_{DL}) [28]. The emission spectra of graphene/SnO_2 QDs composites were recorded under irradiation by 254 nm in the range 300–650 nm as shown in Fig. 4. The I_{UV}, I_{DL}, and (I_{UV}/I_{DL}) ratio values for composites are listed in Table 1. It may be directly observed from table that the defect density increases with the content of graphene. This reflects

SnO_2 QDs are firmly attached to graphene sheets through dangling bonds.

3.2. Gas sensing properties

The capability of a chemiresistor to respond to a particular gas in the presence of other gases is known as selectivity. A comparative plot of sensing responses of chemiresistors to LPG (as a representative of reducing gas) and CO_2 (as a representative of oxidizing gas) is presented in Fig. 5. From Fig. 5 it is seen that the maximum sensing response is observed for LPG as compared to CO_2 gas. The results of selectivity performance of as-synthesized composites show that materials are more selective towards the LPG than CO_2. This may be due to the free energy difference between gas molecules and sensing surface. The free energy that drives the adsorption and chemisorption reaction is the difference in reduction potential between donor and acceptor.

Because the chemiresistors are more selective towards the LPG, further study of gas sensing is carried out using LPG. Fig. 6 shows the sensing response as a function of LPG concentration (ppm) at room temperature. It is seen from Fig. 6 that for each chemiresistor, the response increased with the wt.% of graphene. The plot clearly shows that the sensing response improved in the composite state more than in pristine SnO_2.

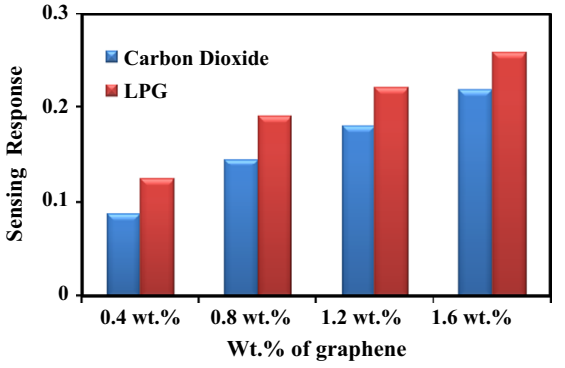

Fig. 5. Comparative gas sensing responses of chemiresistors towards CO_2 and LPG for 50 ppm at room temperature.

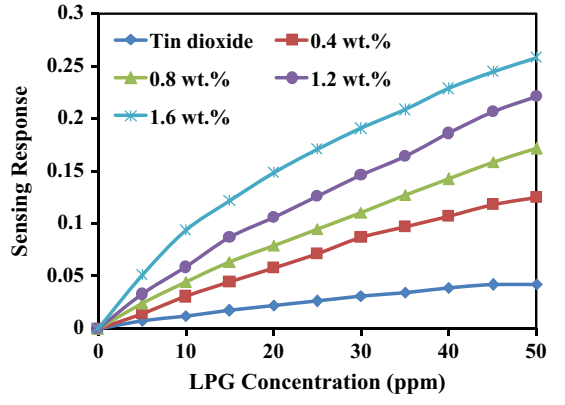

Fig. 6. The variation of sensing response of chemiresistors with the concentration of LPG at room temperature.

The possible reason for increase in sensing response is that at low contents of graphene, electrons mainly transfer due to SnO_2 and electrons follow a hopping mechanism. By contrast, at a high content of graphene, it overlaps on to the SnO_2 QDs and the resistance of graphene is lower than that of SnO_2 QDs. Hence, the adsorption of LPG increases with the wt.% of graphene and SnO_2 played important to make graphene sheets defective. When chemiresistors are exposed to an LPG environment, LPG molecules are adsorbed onto oxygen ions. Therefore, the physical adsorption of LPG on the graphene surface is the dominant sensing mechanism. The plausible sensing mechanism for LPG detection is shown in Fig. 7. The gas sensing action basically depends on the adsorbed oxygen density. As mentioned above, the gas sensing response is related to defects, that is, oxygen vacancies can act as adsorption sites for gas molecules. The reaction for adsorbed oxygen ions are shown in (Eqs.(2)–4) [23].

$$O_2\,(\text{gas}) \rightarrow O_2\,(\text{ads}) \tag{2}$$

$$O_2\,(\text{ads}) + e^- \rightarrow O_2^-\,(\text{ads}) \tag{3}$$

$$O_2^-\,(\text{ads}) + e^- \rightarrow 2O^-\,(\text{ads}) \tag{4}$$

LPG is the composition of CH_4, C_3H_8, C_4H_{10} etc., and these molecules have a tendency to donate electrons to the surface. A powerful odorant, ethanethiol, is added so that leaks can be detected easily. It is an organosulfur compound with the formula CH_3CH_2SH. Humans can detect ethanethiol in minute concentrations as low as one part in 2.8 billion parts of air. Ethanethiol is intentionally added to LPG for detection purposes. Thus, the impact of ethanethiol is not considered in chemiresistive gas sensing [29,30]. When the chemiresistor is exposed to LPG, it interacts with the adsorbed oxygen ions and forms H_2O

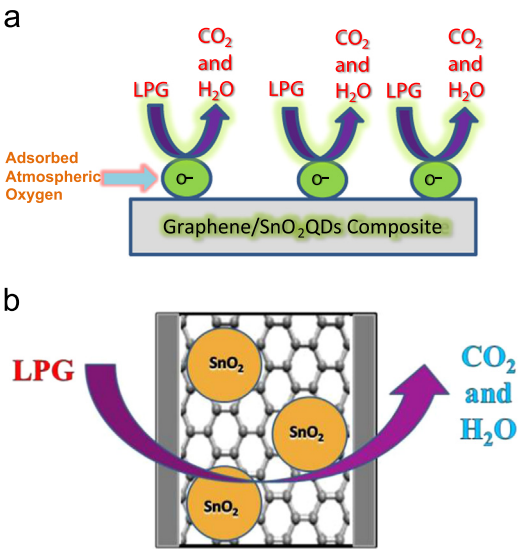

Fig. 7. Plausible sensing mechanism for LPG detection.

and CO_2. The reaction between LPG and adsorbed oxygen ions are represented by (Eqs. (5) and 6) [23].

$$C_nH_{2n+2} + 2O^- (ads) \rightarrow H_2O + C_nH_{2n}: O + e^- \quad (5)$$

$$C_nH_{2n}: O + O^- (ads) \rightarrow CO_2 + H_2O + e^- \quad (6)$$

Fig. 8 shows the sensing response as a function of operating temperature to 30 ppm LPG. It may be observed from Fig. 8 that the response increased up to 423 K. This is the operating temperature for chemiresistors, which is much lower than the autoignition temperature of LPG. This is an important accomplishment of this present work. At higher temperatures, the thermal energy is sufficient to overcome the potential barrier and resulted in a significant increase in electron concentrations for the sensing reaction. The sensing response of semiconductor–oxide-based gas sensors depends on the speed of the chemical reaction on the surface of the particles and the speed of diffusion of the gas molecules to that surface. At lower temperatures, the sensing response is constrained by the speed of the chemical reaction, and at higher temperatures it is constrained by the speed of diffusion of gas molecules. At some transitional temperature, the speed values of the two processes become equal, and at that point the chemiresistor response attained its maximum value [31]. The response value starts to decreases beyond 423 K. This may be due to the desorption of oxygen ions and diffused gas molecules from the sensing surface [23].

As discussed earlier, the defects concentration affects the sensing response significantly. Therefore, the study of sensing parameters as a function of defects density is crucial. It is evident that good correlation exists between the I_{UV}/I_{DL} ratio (defects density) and gas sensing response as a function of wt.% of graphene as shown in Fig. 9. The increase in defects density may be due to the SnO_2 QDs forming dangling bonds with graphene [32]. As the wt.% of graphene increases, more and more graphene sheets come in contact with Sb_2O_3 QDs and are damaged. Thus, the graphene sheets becomes defects rich. This is one of the possible reasons for the increase of the sensing response with the increasing wt.% of graphene.

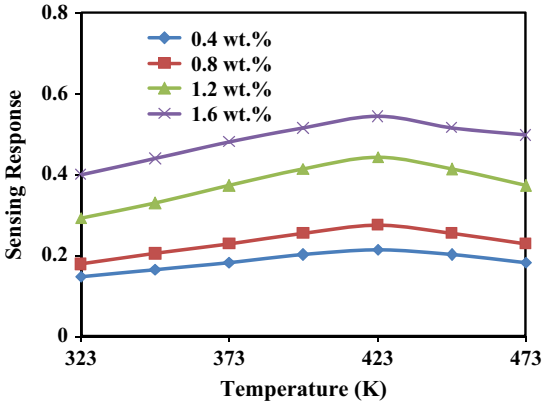

Fig. 8. Chemiresistor response as a function of operating temperature to 30 ppm LPG.

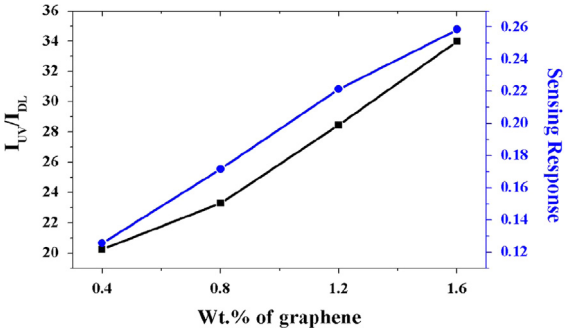

Fig. 9. The variation of defects density (I_{UV}/I_{DL}) ratio and LPG sensing response with graphene content (wt.%).

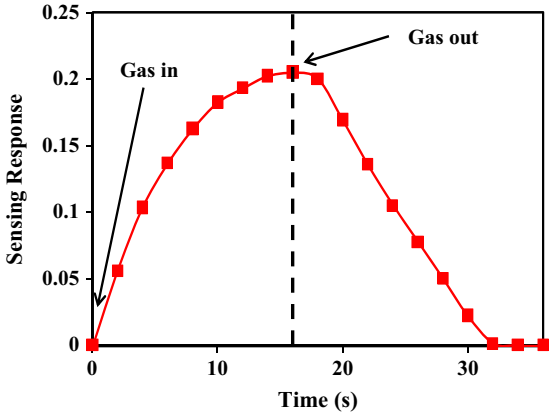

Fig. 10. Transient response of 1.6 wt.% graphene/SnO_2 QDs chemiresistor to 50 ppm LPG.

The sensing response of a chemiresistor depends on the removal of adsorbed oxygen molecules by reacting with a target gas resulting in the generation of electrons. The gas sensing response is related to the defects concentration through the oxygen vacancies, which can act as adsorption sites for atmospheric oxygen [33]. The higher the capability of the surface to receive and oxidize the target gas, the higher the change in conductance of the chemiresistor could be, and, consequently, enhancement of the gas sensing response. As the LPG comprises CH_4, C_3H_8, C_4H_{10}, etc., it interacts with the adsorbed oxygen ions on the surface and undergoes complete oxidation forming water and CO_2 [34].

The transient response characteristic for 1.6 wt.% graphene/SnO_2 QDs chemiresistors to 50 ppm LPG is shown in Fig. 10. For the transient response measurement, the gas was filled into the chamber and the chemiresistor attained its highest stable sensing response value. A fast response of ~16 s for LPG was shown by chemiresistors. The chemiresistor was exposed to air and the time taken by it to reduce its highest value by 90%, is known as the recovery time. For 1.6 wt.% graphene/SnO_2 QDs chemiresistors, the recovery time was ~20 s.

For stability measurements, 1.6 wt.% graphene/SnO_2 QDs chemiresistor responses towards 50 ppm LPG at room temperature was measured for 30 days and are shown

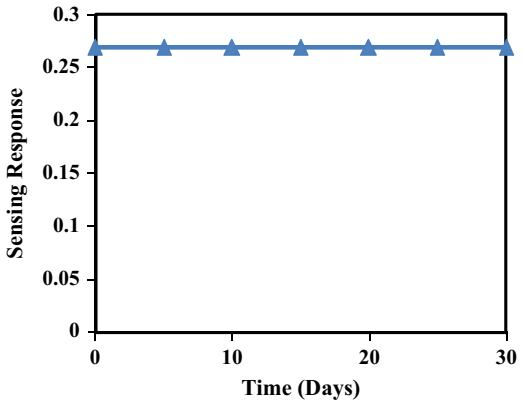

Fig. 11. Stability characteristics of 1.6 wt.% graphene/SnO_2 QDs chemiresistor to 50 ppm LPG.

in Fig. 11. The chemiresistors show a nearly constant response to LPG, indicating good stability.

4. Conclusions

We have successfully demonstrated a chemiresistive gas sensing application of graphene/SnO_2 QDs composites for LPG. The phase composition and structural purity analyzed by XRD showed the formation of the composite. FE-SEM and TEM was used to analyze the morphology of the materials and shows SnO_2 QDs finely anchored on the graphene. The UV-VIS and fluorescence spectroscopy were used to investigate the quantum confinement and defects density, respectively. The 1.6 wt.% graphene/SnO_2 QDs composite chemiresistor is a good candidate for practical use in the detection of LPG as it shows a good sensing response at low operating temperatures, good stability, fast response times and good recovery.

Acknowledgments

The authors are grateful to the Head of the Department of Physics Sant Gadge Baba Amravati University, Amravati for providing the necessary facilities for this study. K.R. Nemade is thankful to Sant Gadge Baba Amravati University, Amravati for financial support through the Late M.N. Kale scholarship (2012).

References

[1] D.S. Dhawale, D.P. Dubal, A.M. More, T.P. Gujar, C.D. Lokhande, Sens. Actuators B 147 (2010) 488–494.
[2] S. Singha, A. Singha, B.C. Yadava, P.K. Dwivedi, Sens. Actuators B 177 (2013) 730–739.
[3] C.K.N. Patel, E.G. Burkhardt, C.A. Lambert, Science 184 (1974) 1173–1176.
[4] M.W. Sigrist, Air Monitoring by Spectroscopic Techniques, J. Wiley & Sons, New York, 1994.
[5] C.L. Yuan, C.P. Chang, Y.S. Hong, Y. Sung, Materials Science-Poland 27 (2009) 509–520.
[6] V. Balouria, S. Samanta, A. Singh, A.K. Debnath, A. Mahajan, R.K. Bedi, D.K. Aswal, S.K. Gupta, Sens. Actuators B 176 (2012) 38–45.
[7] H. Bai, G. Shi, Sensors 7 (2007) 267–307.
[8] K.R. Nemade, S.A. Waghuley, Int J. Modern Physics: Conference Series 22 (2013) 380–384.
[9] M.E. Franke, T.J. Koplin, U. Simon, Small 2 (2006) 36–50.
[10] K.R. Nemade, S.A. Waghuley, AIP Conf. Proc. 1536 (2013) 1258–1259.
[11] B. Thomas, S. Benoy, K.K. Radh, Sens. Actuators B 133 (2008) 404–413.
[12] P. Sun, L. You, D. Wang, Y. Sun, J. Ma, G. Lu, Sens. Actuators B 156 (2011) 368–374.
[13] R.R. Salunkhe, D.S. Dhawale, U.M. Patil, C.D. Lokhande, Sens. Actuators B 136 (2009) 39–44.
[14] J.Y. Patil, M.S. Khandekar, I.S. Mulla, S.S. Suryavanshi, Current Appl. Phys. 12 (2012) 319–324.
[15] C.Y. Choi, I. Hwang, J. Park, K.J. Choi, J. Park, J. Lee, Nanotechnology 19 (2008) 095508–095512.
[16] F. Li, J. Song, H. Yang, S. Gan, Q. Zhang, D. Han, A. Ivaska, L. Niu, Nanotechnology 20 (2009) 455602–455608.
[17] Z. Zhang, R. Zou, G. Song, L. Yu, Z. Chen, J. Hu, J. Mater. Chem. 21 (2011) 17360–17365.
[18] H. Song, L. Zhang, C. He, Y. Qu, Y. Tian, Y. Lv, J. Mater. Chem. 21 (2011) 5972–5977.
[19] X. Wang, X. Cao, L. Bourgeois, H. Guan, S. Chen, Y. Zhong, D. Tang, H. Li, T. Zhai, L. Li, Y.o. Bando, D. Golberg, Adv. Funct. Mater. 22 (2012) 2682–2690.
[20] B. Wang, D. Su, J. Park, H. Ahn, G. Wang, Nanoscale Res. Lett. 7 (2012) 215–222.
[21] P. Lian, X. Zhu, S. Liang, Z. Li, W. Yang, H. Wang, Electrochim. Acta 56 (2011) 4532–4539.
[22] K.R. Nemade, S.A. Waghuley, J. Elec. Mater. 42 (2013) 2857–2866.
[23] K.R. Nemade, S.A. Waghuley, Solid State Sci. 22 (2013) 27–32.
[24] B.C. Yadav, S. Singh, A. Yadav, Appl. Surface Sci. 257 (2011) 1960–1966.
[25] Y. Wu, B. Wang, Y. Ma, Y. Huang, N. Li, F. Zhang, Y. Chen, Nano. Res. 3 (2010) 661–669.
[26] K.R. Nemade, S.A. Waghuley, Results Phys. 3 (2013) 52–54.
[27] J. Archana, M. Navaneethan, T. Prakash, S. Ponnusamy, C. Muthamizhchelvan, Y. Hayakawa, Mater. Lett. 100 (2013) 54–57.
[28] O. Lupan, V.V. Ursaki, G. Chai, L. Chow, G.A. Emelchenko, I. M. Tiginyanu, A.N. Gruzintsev, A.N. Redkin, Sens. Actuators B 144 (2010) 56–66.
[29] Q. Zhang, X. Li, K. Asami, S. Asaoka, K. Fujimoto, Fuel Process. Technol. 85 (2004) 1139–1150.
[30] J. Hernandez, J. Lafuente, O.J. Prado, D. Gabriel, J. Air Waste Manag. Assoc. 63 (2013) 462–471.
[31] T.G. Nenov, S.P. Yordanov, Ceramic Sensors, Technology and Applications, Technomic Publishers, Lancaster, 1996.
[32] Z. Ni, Y. Wang, T. Yu, Z. Shen, Nano. Res. 1 (2008) 273–291.
[33] S. Pati, S.B. Majumder, P. Banerji, J. Alloys Comp. 541 (2012) 376–379.
[34] M.V. Vaishampayan, R.G. Deshmukh, I.S. Mulla, Sens. Actuators B 131 (2008) 665–672.